A New Kinetically Preferable Polymorph of 1-(4′-Cyanobenzyl)pyridinium bis(maleonitriledithiolato)nickelate with Spin-Peierls-type Transition

Article

A new kinetically preferable polymorph of 1-(4'- cyanobenzyl)pyridinium bis(maleonitriledithiolato)nickelate with spin-Peierls type transition

Guo-Jun Yuan, Dong-Sheng Shao, Qiu Ren, Fei-Yan Feng, Hao Yang, Lifeng Wang, and Xiao-Ming Ren

Cryst. Growth Des., **Just Accepted Manuscript** • DOI: 10.1021/acs.cgd.9b01551 • Publication Date (Web): 10 Feb 2020

A new kinetically preferable polymorph of 1-(4′-cyanobenzyl)pyridinium bis(maleonitriledithiolato)nickelate with spin-Peierls type transition

Guo-Jun Yuan,[a,b] Dong-Sheng Shao,[a] Qiu Ren,[a] Fei-Yan Feng,[b] Hao Yang,[a] Lifeng Wang,[c] Xiao-Ming Ren*[a]

[a] State Key Laboratory of Materials-Oriented Chemical Engineering and College of Chemistry and Molecule Engineering, Nanjing Tech University, Nanjing 211816, P. R. China

[b] Key Laboratory of Advanced Materials of Nanjing and Department of Chemistry, Nanjing Xiaozhuang University, Nanjing 211171, P. R. China

[c] Institute for Frontier Materials (IFM), Deakin University, 75 Pigdons Road, Waurn Ponds, Victoria 3216, Australia

Tel.: +86 25 58139476

Email: xmren@njtech.edu.cn

Abstract

A new kinetically preferable polymorph of 1-(4'-cyanobenzyl)pyridinium bis(maleonitriledithiolato)nickelate (β-[CN-Py][Ni(mnt)$_2$]) was achieved and characterized by element microanalysis for C, H and N elements, powder X-ray diffraction (PXRD) and differential scanning calorimetry (DSC) techniques. β-[CN-Py][Ni(mnt)$_2$] shows a magnetostructural phase transition together with a thermal anomaly at ~192 K. In high-temperature phase (HTP), the β-[CN-Py][Ni(mnt)$_2$] crystal belongs to monoclinic space group $P2_1/c$, and its asymmetric unit is comprised of one pair of CN-Py$^+$ and [Ni(mnt)$_2$]$^-$ ions. Both CN-Py$^+$ and [Ni(mnt)$_2$]$^-$ ions form uniform columnar stacks, respectively. In low-temperature phase (LTP), the space group of the crystal is lowered to triclinic *P-1*, its asymmetric unit changes into two pairs of anions and cations, moreover, both stacks of CN-Py$^+$ and [Ni(mnt)$_2$]$^-$ ions are dimerized. β-[CN-Py][Ni(mnt)$_2$] features an S = ½ Heisenberg regular antiferromagnetic (AFM) linear chain system with $|J|$ = 86(9) K in HTP, while a spin gap is opened with Δ = 568 K in LTP. The magnetic phase transition in β-[CN-Py][Ni(mnt)$_2$] shows the spin-Peierls transition characters from the changes of both crystal structures and magnetic natures.

Keywords: Nickel-bis-dithiolene, polymorph, spin-Peierls-type transition, symmetry breaking phase transition

Introduction

Polymorphism means that a solid shows different crystalline forms or crystallized structures, which generally have various thermal stabilities and physicochemical properties but with the same components. A crystallization process includes the nucleation of the first crystallites and the growth of crystalline phase; and the formation of different polymorphs is dependent on the initial nucleation process. Many researchers have made tremendous efforts to deeply understand the polymorphism phenomenon,[1-4] which lead to significant progress being achieved in the crystal engineering of polymorph up to now.[5,6] However, it still remains challenging to predict and control the different forms emerging for a solid at present stage owing to the initial nucleation process being hard surveyed.[7-10]

The crystal structure generally determines the properties of a matter, and thus, different polymorphisms often show distinct functionalities, probably leading to different technological applications.[11,12] In a molecule crystal, the molecule packing fashion is strongly influenced by intermolecular weak interactions, including π…π stacking, C-H…π, H-bonding or S…S, S…N, S…C, halogen…halogen and van der Waals interactions etc. Since the different arrangements show small energy differences in molecule crystals, the polymorphism is a common phenomenon, especially, in the crystals with planar π-conjugated molecule architectures, e.g., a charge-transfer salt [4'-CF_3bzPy][Ni(mnt)$_2$], in which 4'-CF_3bzPy$^+$ and mnt^{2-} correspond respectively to 1-(4'-trifluoromethylbenzyl)pyridinium and maleonitriledithiolate, crystallizes in two types of polymorphs,[13, 14] amongst them one crystal form shows mixed stack of anion and cation with a hysteretic magnetic transition at 159/208 K on cooling/heating;[13] another crystal form has separately stacks of anions and cations, undergoing two hysteretic magnetic phase transitions in a narrow temperature region (190–217 K).[14] The molecule materials with hysteretic effect show intrinsically memory effect to have promising applications in the areas of information storage etc.[15-18]

Spin-Peierls transition is an interesting phenomenon in the low-dimensional spin systems, theoretically predicted by R. E. Peierls in 1955.[19] A one-dimensional (1D)

Heisenberg S = ½ regular AFM linear chain is a thermodynamic unstable spin system with respect to the dimerized chain, the spin chains dimerize at a certain temperature and at this transition the matter undergoes a second-order transition to reach a singlet ground state with a magnetic gap, moreover, the magnetic gap progressively increases with lowering temperature and reaches to the maximum at the absolute zero Kelvin. The driving force of spin-Peierls transition is magnetic-lattice interaction. Experimentally, a spin-Peierls transition was firstly found in a charge-transfer salt, [TTF][$CuS_4C_4(CF_3)_4$] where TTF^+ = tetrathiafulvalinium and $[S_2C_2(CF_3)_2]^{2-}$ = cis-(1,2-perfluoromethylethylene-1, 2-dithiolato).[20] Since then, several families of charge-transfer salt-based[21-27] and inorganic[28-30] spin-Peierls systems have been reported in succession.

In previous study, we harvested one crystal form of charge-transfer salt [CN-Py][$Ni(mnt)_2$], where the $CN\text{-}Py^+$ denotes 1-(4'-cyanomethylbenzyl)pyridinium and this crystalline form is labeled as α-[CN-Py][$Ni(mnt)_2$].[31] α-[CN-Py][$Ni(mnt)_2$] features a 1D Heisenberg S = ½ regular AFM chain system, but shows complicated magnetic behaviors, including that a magnetic transition occurs at ~190 K, leading to spin gap ($\Delta \approx 614$ K) opening in LTP, and the canted spin anti-ferromagnetism appears in the low temperature at 2 K with a clearly magnetic hysteresis. However, the temperature dependent single crystal structure and PXRD analyses demonstrated that no crystal structure phase transition undergoes at ~190 K. Moreover, there is no thermal anomaly at ~190 K in the DSC plot. The observation that a Heisenberg S = ½ regular AFM chain system with a magnetic transition and a spin gap is rather interesting phenomenon.[31]

In this work, we further obtained a new polymorph of [CN-Py][$Ni(mnt)_2$], which shows segregate cation and anion stacks with a spin-Peierls-type transition at ~192 K, and this new crystal form is labeled as β-[CN-Py][$Ni(mnt)_2$]. The calculation for the total energy of per unit cell revealed that α-[CN-Py][$Ni(mnt)_2$] is more stable phase in thermodynamics, while β-[CN-Py][$Ni(mnt)_2$] is kinetically preferred form. In addition, the crystal structures and magnetic behaviors in both HTP and LTP are explored for β-[CN-Py][$Ni(mnt)_2$] in detail.

Experimental section

Chemicals and materials

The reagents and chemicals used in this study were purchased from commercial sources. The starting material, Na_2mnt,[32] [CN-Py]Br and $[CN\text{-}Py]_2[Ni(mnt)_2]$[31] were prepared following the literature approaches.

Formation and growth of β-[CN-Py][Ni(mnt)$_2$] Crystals

The I_2 (150 mg, 0.59 mmol) dissolved in 10 cm^3 methanol was added drop-by-drop into the methanol solution (20 cm^3) containing $[CN\text{-}Py]_2[Ni(mnt)_2]$ (730 mg, 1.0 mmol), and this mixture was stirred for 15 minutes and then stood overnight. The black microcrystals were filtered off. Noticeably, these microcrystals were not washed using any solvent, but directly dissolved in MeCN/Me_2CO to give the solution, and such type of solution was evaporated at ambient temperature for 6-8 days to yield β-$[CN\text{-}Py][Ni(mnt)_2]$ crystals, and these crystals are suitable to be used for the collection of single crystal X-ray diffraction data. Otherwise, only α-$[CN\text{-}Py][Ni(mnt)_2]$ crystals were obtained. The β-$[CN\text{-}Py][Ni(mnt)_2]$ crystals were separated using suction, washed with small amount of methanol and dried under vacuum at room temperature. Yield: ca. 87% calculated on the reactant $[CN\text{-}Py]_2[Ni(mnt)_2]$. Elemental microanalysis calculated for $C_{21}H_{11}N_6NiS_4$: C, 47.21; H, 2.08; N, 15.73%. Found: C, 47.14; H, 2.05; N, 15.67%.

The phase purity of both α-$[CN\text{-}Py][Ni(mnt)_2]$ and β-$[CN\text{-}Py][Ni(mnt)_2]$ was examined by PXRD technique (ref. Figure S1).

Chemical characterization and physical measurements

Elemental analyses (C, H and N) were performed with an Elementar Vario EL III analytical instrument. PXRD data were collected on a Bruker D8 Advance powder diffractometer operating at 40 kV and 40 mA for Cu Kα radiation with λ = 1.54018 Å. Polycrystalline samples were used for this measurement and the 2θ scan ranges from 5 to 50° with 0.02 °/step and 1.2 s/step. DSC measurement was carried out using a DSC Q2000 V24.10 Build 122 for polycrystalline sample in 100-298 K, with a temperature scanning rate of 10 $K \cdot min^{-1}$. Magnetic susceptibility data were recorded for polycrystalline samples in 1.8-300 K using a Quantum Design MPMS-5S

superconducting quantum interference device (SQUID) magnetometer and the molar magnetic susceptibility χ_m of β-[CN-Py][Ni(mnt)$_2$] is calculated using one [Ni(mnt)$_2$]$^-$ anion per formula unit and the diamagnetism was not removed from the experimental data.

X-ray single crystallography

The single-crystal X-ray diffraction data were collected at 296 and 105 K for β-[CN-Py][Ni(mnt)$_2$], respectively, utilizing the graphite monochromated Mo Kα (λ = 0.71073 Å) on a Bruker-SMART CCD area detector. Diffraction data reductions and absorption corrections were made using the SAINT and SADABS software packages,[33] respectively. Crystal structures were solved by means of direct method using the SHELXL-2014/7 software package,[34] and the non-hydrogen atoms were anisotropically refined using the full-matrix least-squares method based on F^2. All hydrogen atoms were placed at their calculated positions, which were refined using the riding model on the bound atoms. The crystal of β-[CN-Py][Ni(mnt)$_2$] is easily cracked when it was cooled from HTP to LTP. Fortunately, the single-crystal X-ray diffraction data were collected for β-[CN-Py][Ni(mnt)$_2$] at 105 K as the single crystal was slowly cooled at a rate of 1 Kelvin per ten minuses and the crystal structure in LTP was then determined. The final cif file was checked by TwinRotMat in Platon program,[35] indicating that the high quality single crystal in HTP changes into a (non)Merohedral Twinning in LTP, with total number of 9981 reflections in HKLF 5 file, in which the number of Twin Contribution reflections are 2039 and the estimated BASF Line = 0.35. The (non)Merohedral Twinning leads to the refinement parameters, such as R_σ, R_1 and wR_2 etc. being slight high in LTP.

The single crystal X-ray diffraction data collection, structure refinements and crystallography are summarized in Table 1 for β-[CN-Py][Ni(mnt)$_2$] in both HTP and LTP. For the sake of benefiting comparison, the single crystal X-ray diffraction data were re-collected for α-[CN-Py][Ni(mnt)$_2$] at 296 K, and the details on the diffraction data collection, structure refinements and crystallography in this work and in the literatures[31] are summarized in Tables S1 and S2.

Table 1: Crystallographic data and refinement parameters for β-[CN-Py][Ni(mnt)$_2$] in HTP and LTP

	HTP	LTP
Temp. / K	296(2)	105(2)
Wavelength / Å	0.71073	0.71073
Formula	$C_{21}H_{11}N_6NiS_4$	$C_{21}H_{11}N_6NiS_4$
Formula weight	534.31	534.31
Space group	*P2$_1$/c*	*P-1*
CCDC no.	1427934	1903767
Crystal system	Monoclinic	Triclinic
a / Å	12.1780(17)	7.0610(5)
b / Å	26.818(4)	12.1473(9)
c / Å	7.2530(9)	26.647(2)
α / °	90	88.533(6)
β / °	103.380(4)	86.386(6)
γ / °	90	76.877(7)
V /Å^3 /Z	2304.5(5)	2221.3(3)
ρ / g·cm^{-1}	1.540	1.598
F(*000*)	1084	1084
Abs.coeff. / mm^{-1}	1.226	1.272
θ Range for data collection (°)	1.88-27.60	2.86-28.84
Index ranges	$-15 \le h \le 15$ $-34 \le k \le 32$ $-9 \le l \le 9$	$-6 \le h \le 9$ $-16 \le k \le 15$ $-32 \le l \le 36$
R_{int}	0.0841	0.0797
Independent reflect. /restraints/parameters	5323/0/290	9981/0/257
Refinement method	The least square refinement on F^2	
Goodness of fit on F^2	0.987	1.156
R_1, wR_2 [$I>2\sigma$(I)]	$R_1 = 0.0474$ $wR_2 = 0.0811$	$R_1 = 0.2362$ $wR_2 = 0.5495$
R_1, wR_2 [all data]	$R_1 = 0.1279$ $wR_2 = 0.0993$	$R_1 = 0.2659$ $wR_2 = 0.5638$
Residual / e·Å^{-3}	0.265/-0.343	0.397/-3.485

$R_1 = \sum||F_o| - |F_c||/|F_o|$, $wR_2 = [\sum w(\sum F_o^2 - F_c^2)^2/\sum w(F_o^2)^2]^{1/2}$

Crystal structure optimization

Crystal structure optimizations and the total energy calculations were performed for both α-[CN-Py][Ni(mnt)$_2$] and β-[CN-Py][Ni(mnt)$_2$] in HTP. All calculations

were made in the Density Functional Theory (DFT) framework using the Cambridge Sequential Total Energy Package (CASTEP) module,[36,37] and the Generalized Gradient Approximation (GGA) with Perdew-Burke-Ernzerhof (PBE)[38] exchange-correlation functional is used for the calculations. The starting crystal structures used for the geometry optimization were directly taken from the single crystal data of α-[CN-Py][Ni(mnt)$_2$] and β-[CN-Py][Ni(mnt)$_2$] at 296 K, respectively; the coordinates of all atoms are optimized but the unit cell is fixed. The bond lengths and bond angles in both moieties of anion and cation, from the optimized crystal structures, are summarized in Tables S3-S6 for α-[CN-Py][Ni(mnt)$_2$] and β-[CN-Py][Ni(mnt)$_2$], which match well with the corresponding values acquired from the single crystal X-ray diffraction analyses for α-[CN-Py][Ni(mnt)$_2$] and β-[CN-Py][Ni(mnt)$_2$] at 296 K. The total energy per unit cell was then calculated based on the optimized crystal structures. In the DFT calculations, the electrons in the Ni ($3d^8 4s^2$), S ($3s^2 3p^4$), N($2s^2 2p^3$) and C ($2s^2 2p^2$) orbitals are treated as the valence electrons, the quality of calculations was set to fine as implemented in the CASTEP and other calculating parameters were set as the default values in the CASTEP code.

Results and discussion

Crystal structures of β-[CN-Py][Ni(mnt)$_2$]

β-[CN-Py][Ni(mnt)$_2$] crystallizes in monoclinic system with space group $P2_1/c$ in HTP. As displayed in Figure 1a, an asymmetric unit is comprised of one pair of anion and cation. The [Ni(mnt)$_2$]$^-$ anion shows planar structure and the CN-Py$^+$ cation displays the Λ-shaped conformation of molecule. As listed in Table S1, the bond lengths and bond angles in both cation and anion are comparable to the values in α-[CN-Py][Ni(mnt)$_2$].[31] The mean-molecule plane in the [Ni(mnt)$_2$]$^-$ moiety, defined through four coordination sulfur atoms, is roughly parallel to the phenyl ring in the CN-Py$^+$ with a dihedral angle of 10.2° at 296 K in HTP. The orientation of long molecule axis in the anion is nearly parallel to the C-C≡N part in the cation (ref. Figure 1b and 1c), such a type of relative arrangement between the cation and anion in β-[CN-Py][Ni(mnt)$_2$] is distinction from that in α-[CN-Py][Ni(mnt)$_2$], where the orientation of long molecule axis in the anion is roughly perpendicular to the C-C≡N

part in the cation (ref. Figures 1e and 1f).

As depicted in Figure 1b, the cations and anions are arranged into segregated stacks along the *c*-axis; each stack has two cations or two anions per unit (Figure 1c). The cation and anion stacks show alternative arrangement along *a*- and *b*-axes, leading to each anion stack being enclosed by four cation stacks and vice versa (ref. Figure 1b). The relative slippage are observed in an anion stack along the long molecule axis of anion and slight rotation between two superimposed anions, and this type of arrangement offers an efficient way to reduce the electrostatic repulsions between the adjacent $[Ni(mnt)_2]^-$ ions. The adjacent $[Ni(mnt)_2]^-$ ions show the exact equidistances of Ni…Ni, S(i)…S(i), N(i)…N(i) and C(i)…C(i) (i = 1-4) within a stack.[39]

In a stack, the adjacent cations are arranged in a boat-type manner, the phenyl rings are nearly parallel to each other, and the CN groups in the phenyl rings point towards the pyridyl ring of the adjacent cation, indicating that there may exists the CN…π interaction[40] between the CN groups with lone electrons pair in the phenyl rings and neighboring electron-deficient pyridyl rings. The adjacent cations have the exact equal distance of centroid-to-centroid of the phenyl rings in a cation stack (Figure S2) for the same reason as that described in the case of anion stack.[39] In addition, it is clearly that there exist charge-assisted hydrogen bonds between cations and anions, which is shown in Figure 1d.

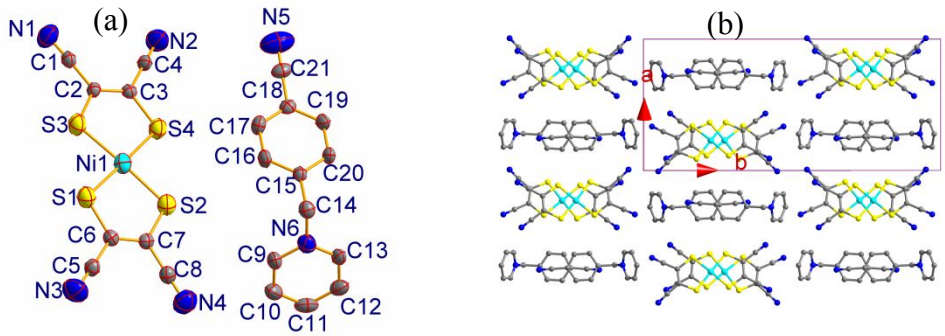

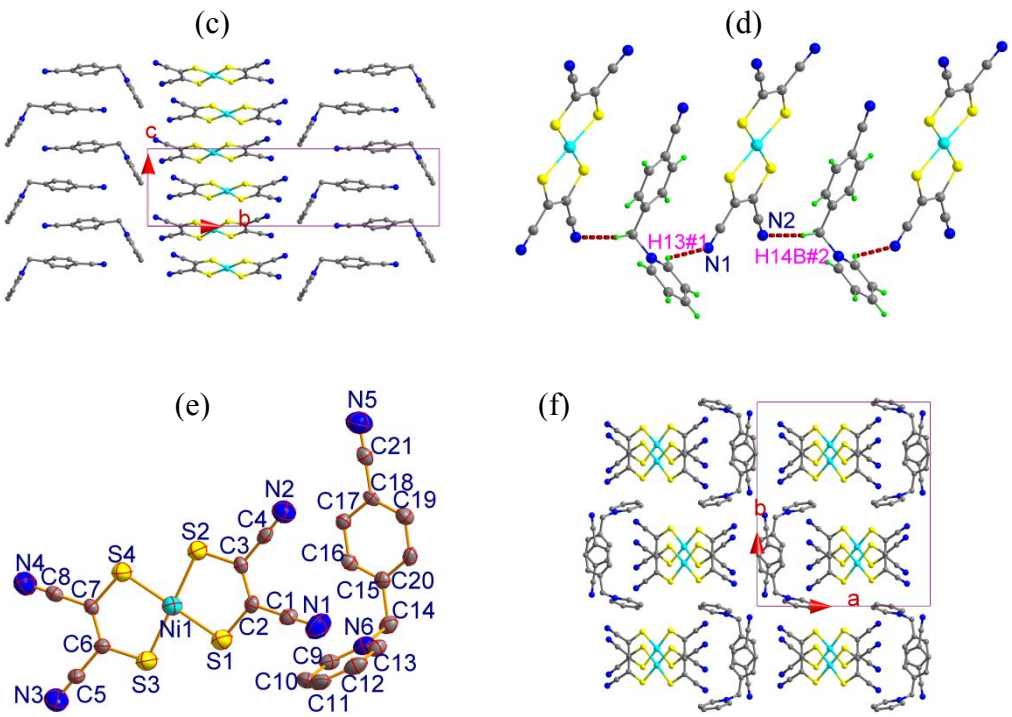

Figure 1: (a) An asymmetry unit containing the labeling of non-hydrogen atoms and the displacement ellipsoids set at the 50% probability level (b, c) packing structures viewed along *c*- and *a*-axis (d) charge-assisted hydrogen bonds between cations and anions in the crystal structure of β-[CN-Py][Ni(mnt)$_2$] at 296 K in HTP. (e) An asymmetry unit with labeling of non-hydrogen atoms and the displacement ellipsoids set at the 50% probability level and (f) packing structure viewed along *c*-axis in α-[CN-Py][Ni(mnt)$_2$] at 296 K in HTP.

A structure phase transition undergoes at ~192 K in β-[CN-Py][Ni(mnt)$_2$], and the details will be discussed in the next section. From HTP to LTP, the space group degrades from $P2_1/c$ to *P-1*, indicating that the phase transition occurring in β-[CN-Py][Ni(mnt)$_2$] shows the symmetry broken character from the macroscopic point of view, while the Z value remains the same (Z = 4) as that in HTP. Space group $P2_1/c$ corresponds to the crystallographic point group C_{2h}, which has four symmetry elements (*E*, C_2, *i* and σ_h), and space group *P-1* corresponds to the crystallographic point group C_i with two symmetry elements (*E* and *i*). From HTP to LTP, both the two-fold screw axis and the glide plane disappear, and this leads to the molecules (anions/cations) related by the two-fold screw axis and the glide plane being

difference in a unit cell in LTP, accordingly, an asymmetric unit changes from one pair of cation and anion in HTP to two pairs of cations and anions in LTP (Figure 2). The bond lengths and bond angles in the cation and the anion in LTP are rather similar to those in HTP, demonstrating that the symmetry broken structure phase transition only changes the packing structure but not affect the molecule structures of both anion and cation in β-[CN-Py][Ni(mnt)$_2$]. Interestingly, a magnetic phase transition occurs at ~190 K in α-[CN-Py][Ni(mnt)$_2$],[31] nevertheless, the space groups are the same ($P2_1/c$) in the phases below and above the critical temperature of magnetic phase transition, moreover, as shown in Figure S3, both cation and anion stacks still maintain regular in LTP, and no crystal structure phase transition is related to the magnetic phase transition.

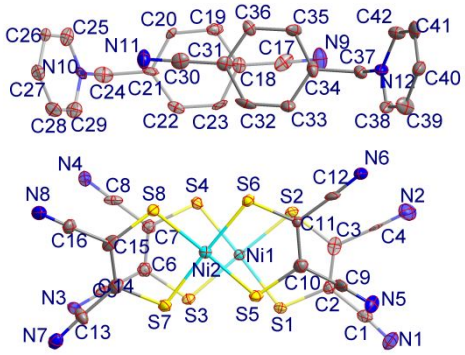

Figure 2: An symmetry unit of β-[CN-Py][Ni(mnt)$_2$] with the labeling of non-hydrogen atoms and displacement ellipsoids set at the 50% probability level at 105 K in LTP.

The symmetry-broken phase transition results in the distortion of both anion and cation stacks, and the alteration of stacks can be found from the characteristic interatom separations, such as the Ni…Ni (denoted as a1 and a2), S…S (represented as b1-b8) and Ni…S (indicated as c1-c8) distances between the adjacent anions in a stack (ref. Figure 3a and Table 1); the centroid-to-centroid distances between the adjacent phenyl rings (denoted as d1 and d2) and the distances of the CN group to the center of pyridyl ring (illustrated as h1 and h2) in a stack (ref. Figure 3b and Table 1) as well as the charge-assisted hydrogen bond distances between the cations and the

anions (ref. Figure 4 and Table 3). Since α-[CN-Py][Ni(mnt)$_2$] and β-[CN-Py][Ni(mnt)$_2$] phases exhibit different stacking structures, as depicted in Figure 4 and Figure S4, they show diverse charge-assisted hydrogen bond networks constructed between anions and cations.

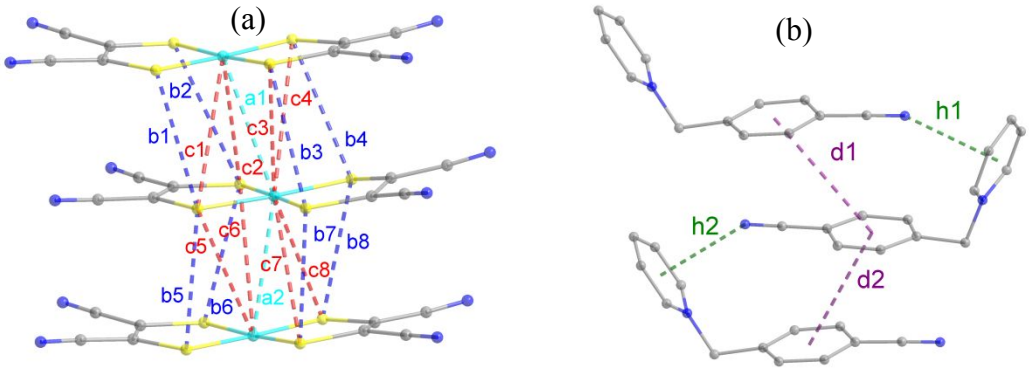

Figure 3: Characteristic distances which demonstrate the distortions of anion and cation stacks in β-[CN-Py[Ni(mnt)$_2$] from HTP to LTP (a) the Ni…Ni, Ni…S and S…S separations in an anion stack (b) the centroid-to-centroid separations of neighboring phenyl rings and the distances of CN group to the centroid of pyridyl ring in a cation stack.

Table 2: Comparison of characteristic interatomic distances in an anion stack and in a cation stack in β-[CN-Py[Ni(mnt)$_2$] in both HTP and LTP

	Distance / Å			Distance / Å	
	HTP(296 K)	LTP (105 K)		HTP(296 K)	LTP (105 K)
a1	3.833	3.752	c2	4.164	3.604
a2	3.833	3.555	c3	3.958	3.600
b1	3.996	3.637	c4	3.830	4.253
b2	3.673	3.919	c5	3.958	3.648
b3	3.958	3.779	c6	3.830	4.195
b4	3.830	3.878	c7	3.628	4.079
b5	3.958	3.548	c8	4.164	3.601
b6	3.830	3.586	d1	4.382	4.470
b7	3.996	3.420	d2	4.382	4.144
b8	3.673	3.629	h1	3.163	3.151
c1	3.628	4.089	h2	3.163	3.023

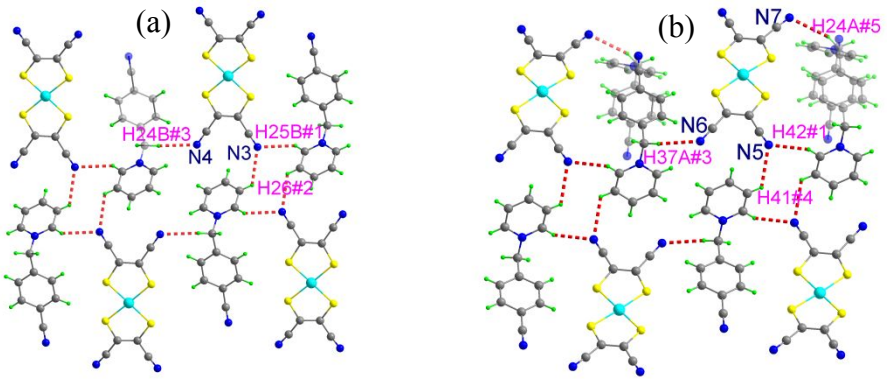

Figure 4: Charge-assisted H-bonds (a) between Ni1 anions and N9 cations (b) between Ni2 anions and N11 cations in β-[CN-Py[Ni(mnt)$_2$] in LTP (symmetry codes: #1 = x, -1+y, z; #2 = 1-x, 1-y, -z; #3 = -1+x, y, z; #4 = -x, 1-y, 1-z; #5 = -1+x, -1+y, z).

Table 3: The atom pairs and the interatomic distances in the charged-assisted H-bonds between the cations and the anions in β-[CN-Py][Ni(mnt)$_2$] in both HTP and LTP

HTP at 296 K		LTP at 105 K	
Atom pair	Distance / Å	Atom pair	Distance / Å
N1…H13#1	2.635	N3…H25B#1	2.613
N2…H14#2	2.736	N3…H26#2	2.635
		N4…H24B#3	2.623
		N5…H42#1	2.541
		N5…H41#4	2.670
		N6…H37A#3	2.604
		N7…H24A#5	2.667
Symmetry codes: #1 = -1+x, 0.5-y, -0.5+z; #2 = x, 0.5-y, 0.5+z		Symmetry codes: #1 = x, -1+y, z; #2 = 1-x, 1-y, -z; #3 = -1+x, y, z; #4 = -x, 1-y, 1-z; #5 = -1+x, -1+y, z	

Selectivity of crystalline phase formation and growth

Both α-[CN-Py][Ni(mnt)$_2$] and β-[CN-Py][Ni(mnt)$_2$] crystals are achievable by means of solvent evaporation the solution of [CN-Py][Ni(mnt)$_2$] in MeCN/Me$_2$CO at ambient condition. It is worth pointing out that, merely α-[CN-Py][Ni(mnt)$_2$] crystals were obtained if the pure sample of [CN-Py][Ni(mnt)$_2$] was used to prepare the solution for crystals growth; the formation and growth of β-[CN-Py][Ni(mnt)$_2$] crystals are available only using the solution of [CN-Py][Ni(mnt)$_2$] in MeCN/Me$_2$CO,

which was made by directly using the microcrystalline sample of [CN-Py][Ni(mnt)$_2$] freshly prepared by I_2 oxidizing [CN-Py]$_2$[Ni(mnt)$_2$], most importantly, not washed by any solvent. This finding demonstrates that some unknown species, as the structure directing agent, plays a crucial role in the nucleation process of β-[CN-Py][Ni(mnt)$_2$] crystals. The unknown structure directing agent is probably one of the ions in the solution, including I^-, I_3^-, CN-Py$^+$ or others. To understand what is the mystical structure directing agent in the formation of β-[CN-Py][Ni(mnt)$_2$] crystals, we re-dissolved the pure β-[CN-Py][Ni(mnt)$_2$] crystals in MeCN/Me_2CO to get the solution, meanwhile, a small amount of [CN-Py]I or [CN-Py]I_3 was added in the solution. Unfortunately, all of the crystals, grew by evaporating the mentioned-above solution at ambient condition, are in α-[CN-Py][Ni(mnt)$_2$] phase.

To gain deeper insight into the selectivity of crystalline phases, the crystal structures of both α-[CN-Py][Ni(mnt)$_2$] and β-[CN-Py][Ni(mnt)$_2$] phases were theoretically optimized using the CASTEP three-dimensional periodic system computational package, while the unit cell parameters were fixed; and the starting crystal structure models were directly taken from the single crystal X-ray diffraction data of both α-[CN-Py][Ni(mnt)$_2$] and β-[CN-Py][Ni(mnt)$_2$] at 296 K. As listed in Tables S3-S6, the bond lengths and bond angles in the anion and cation moieties obtained from structure optimization are in agreement well with those found from single crystal structures of both α-[CN-Py][Ni(mnt)$_2$] and β-[CN-Py][Ni(mnt)$_2$] at 296 K. On basis of the optimized crystal structures, the whole energy of per unit cell was calculated for α-[CN-Py][Ni(mnt)$_2$] (–30065.05 eV) and β-[CN-Py][Ni(mnt)$_2$] (–30064.56 eV), demonstrating that the α-[CN-Py][Ni(mnt)$_2$] phase is thermodynamically stable crystal form and the β-[CN-Py][Ni(mnt)$_2$] phase is kinetically favorable one. The energy difference between two polymorphs is 11.82 kJ mol^{-1}, indicating that two polymorphs show small energy difference.

Magnetic and phase transition features

Plot of χ_m vs. T is depicted in Figure 5a for β-[CN-Py][Ni(mnt)$_2$], where χ_m denotes the molar magnetic susceptibility with one [Ni(mnt)$_2$]$^-$ anion per formula unit and the diamagnetic susceptibility was not deducted from the experimentally

magnetic susceptibility. In the χ_m vs. T plot of β-[CN-Py][Ni(mnt)$_2$], a magnetic phase transition occurs at ~192 K, which is near to the thermal anomaly peak temperature of ~193 K in DSC plot upon cooling (Figure 5b). It should be mentioned that no thermal anomaly occurs around the critical temperature of magnetic transition (which DSC plot is depicted in Figure S5).[31] Below T_C, the magnetic susceptibility reduces sharply and exponentially on cooling, displaying the magnetic character of a spin gap system, and reaches to the minimum (-4.04×10^{-4} emu mol^{-1}) at ~90 K and then rises again during the further cooling process. β-[CN-Py][Ni(mnt)$_2$] shows negative magnetic susceptibility in a wide of temperature range in LTP, demonstrating that the symmetry broken structure phase transition leads to the formation of big spin gap between the singlet ground state and the triplet magnetic excited state, as a result, the Curie-Weiss type paramagnetic susceptibility in 2–90 K contributes mainly from the diamagnetism of atoms core and the paramagnetism of magnetic impurity.

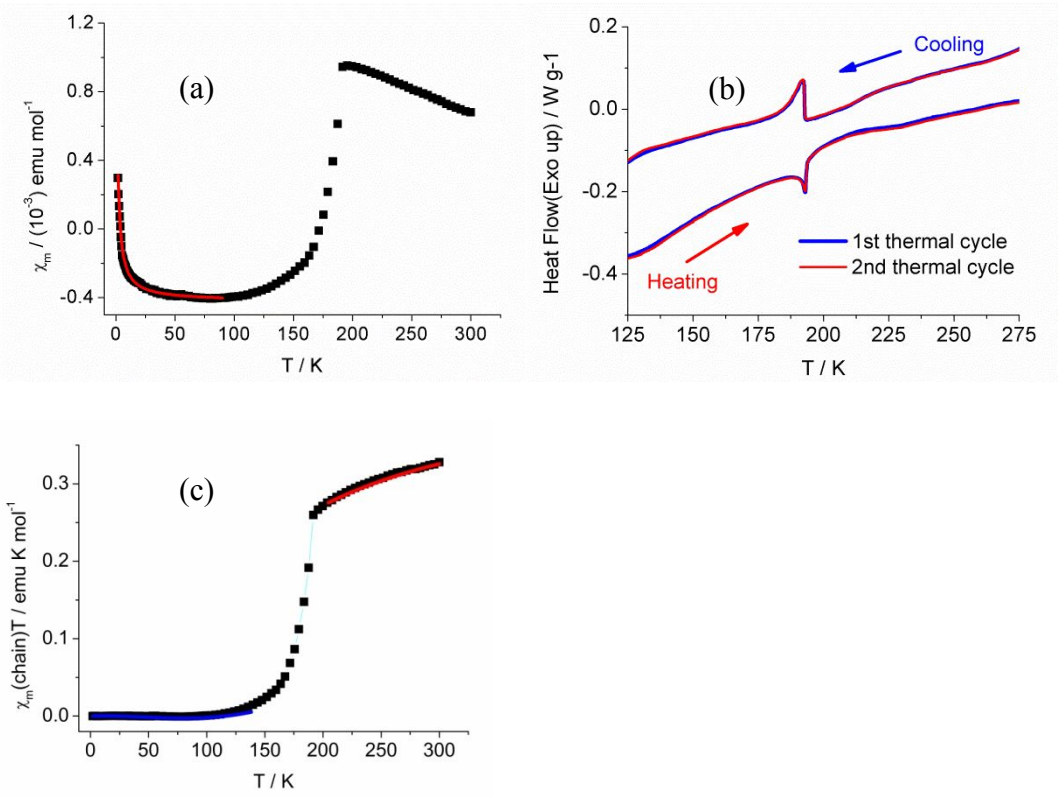

Figure 5: (a) Plot of χ_m vs. T (black squares: experimental data; red line: theoretically reproduced curve using fitted parameters and the details referred to the main text) and

(b) DSC plots in two heating-cooling cycles (c) plot of χ_m(chain)T vs. T (black squares: experimental data; red lines: theoretically reproduced plots using fitted parameters and the details referred to the main text) for β-[CN-Py][Ni(mnt)$_2$].

The Eq. (1), including the atoms core diamagnetism and the magnetic impurity paramagnetism, was firstly used for analyzing the variable temperature magnetic susceptibilities in 2-90 K, and the best fit produced the Curie constant C = 1.83(4)×10^{-3} emu K mol^{-1}, the Weiss constant θ = –0.50(7) K and χ_0 = –4.21(2)×10^{-4} emu mol^{-1}. The amount of S = ½ uncoupled magnetic impurity, arose from the lattice defects, is estimated to be ~0.49% for β-[CN-Py][Ni(mnt)$_2$] from the fitted Curie constant. Too small Weiss constant demonstrates that the magnetic coupling between the lattice defects is really neglectable, and the χ_0 term is close to the diamagnetic susceptibility of β-[CN-Py][Ni(mnt)$_2$], which is estimated from tablet Pascal' constants, indicating that the temperature-independent magnetic susceptibility arises mainly from the atoms core diamagnetism.

$$\chi_m = \frac{C}{T-\theta} + \chi_0 \qquad (1)$$

Since a phase transition does not alternate the lattice defects and the diamagnetism of atoms core, the paramagnetic susceptibility χ_m(chain), contributed from the 1D S = ½ [Ni(mnt)$_2$]$^-$ stack, in both LTP and HTP is achieved by subtracting the diamagnetism and magnetic impurity from the experimental χ_m term. The χ_m(chain)T as a function of temperature is then plotted in Figure 5c. In HTP, the χ_m(chain)T value gradually reduces as the temperature decreases, revealing the existence of AFM coupling between the nearest neighboring spins within the S = ½ [Ni(mnt)$_2$]$^-$ stack, and the χ_m(chain)T value at 300 K is ~0.328 emu K mol^{-1}, which is slight less than 0.375 emu K mol^{-1} calculated from an isolated S = ½ spin-only system. In LTP, the χ_m(chain)T value is close to zero at the temperatures below 90 K, indicating that the ground state is nonmagnetic singlet state.

In the S = ½ Heisenberg alternating linear chain system, the spin Hamiltonian is written as

$$\hat{H} = -2J\sum_{i=1}^{n/2}(\hat{S}_{2i-1}\hat{S}_{2i} + \alpha\hat{S}_{2i}\hat{S}_{2i+1}) \qquad (2)$$

where the symbol J represents the magnetic exchange constant between a spin and its left neighbor and αJ represents the magnetic exchange constant between a spin and its right neighbor. For an AFM coupling system (J < 0 and 0 ≤ α ≤ 1), extremely, the alternating linear chain model is simplified to the dimer model when α = 0 and changed to the uniform linear-chain model if α = 1.[41-43] Deduced from the spin Hamiltonian in Eq. (2), the χ_m(chain) as a function of temperature in a Heisenberg S = ½ AFM linear chain, deduced from the cluster approach, can be written in the form below,

$$\chi_m(chain) = \frac{Ng^2\mu_B^2}{k_BT} \cdot \frac{A + BX + CX^2}{1 + DX + EX^2 + FX^3} \qquad (3)$$

in Eq. (3), $X = |J|/k_BT$, and one set of parameters A-F is valid for the regular linear spin chain when $k_BT/|J| \geq 0.5$, $J \leq 0$,[42] $k_BT_{max}/|J| = 1.282$ and $\chi_{max}|J|/Ng^2\mu_B^2 = 0.07346$;[43] in the case of the irregular linear spin chain, two sets of A-F are valid when $k_BT/|J| \geq 0.5$, $J \leq 0$, amongst them, one set of parameters A-F is usable in the case of 0 ≤ α ≤ 0.4 and another one is valid for 0.4 < α ≤ 1.0.[42,43]

On the basis of the crystal structure and magnetic susceptibility analysis in HTP, the magnetic behavior in HTP was analyzed using the magnetic coupling model of a regular S = ½ Heisenberg AFM linear chain, and the best fit for the χ_m(chain) data in 203.7-300 K gave the parameters of J = –86(9) K with g = 2.2 fixed. The theoretically reproduced χ_m(chain)-T plot is presented in Figure 5c (red line), which matches with the experimental data.

In LTP, the magnetic susceptibility of chain was fitted using the S = ½ Heisenberg alternating linear chain model, and the best fits for the χ_m(chain) data in 1.99-139.7 K yielded the parameters of the averaged J = –379(8) K, the alternating constant α = 0.190(1) with g = 2.2 fixed. The theoretically produced χ_m(chain)-T plot is displayed in Figure 5c (blue line), which is in agreement with the experimental data. The δ constant in the alternating chain in LTP is calculated as $\delta = (1-\alpha)/(1+\alpha) \approx 0.681$, and the spin gap was further estimated as 568 K using the equation of $\Delta(\delta) \approx 2|J|\delta^{3/4}$.[44]

The analyses of both crystal structure and magnetic property revealed that β-[CN-Py][Ni(mnt)$_2$] is a 1D Heisenberg S = ½ AFM linear chain system, and the magnetic transition at ~192 K is a spin-Peierls-type transition, but not a Peierls transition, and the alternating current conductivity measurement further supports this conclusion. As shown in Figure S6, the plots of conductivity against temperature indicate that the β-[CN-Py][Ni(mnt)$_2$] phase not only has rather low conductivity, but also shows no sizable conductivity change around the critical temperature of magnetic transition (i.e., no metal to insulator transition), therefore, the β-[CN-Py][Ni(mnt)$_2$] phase is a magnetic insulator. Additionally, in previous study for a spin-Peierls compound, [NO_2-Py][Ni(mnt)$_2$] (NO_2-Py^+ represents 1-(4-nitrobenzyl)pyridinium) with spin-Peierls transition temperature of ~182 K,[45,46] we found that the nonmagnetic compound, [NO_2-Py][Au(mnt)$_2$], shows the same structure as that of spin-Peierls compound [NO_2-Py][Ni(mnt)$_2$] in HTP, however, no structure phase transition occurs in [NO_2-Py][Au(mnt)$_2$] even at ~100 K, demonstrating that the symmetry-broken structure phase transition observed in [NO_2-Py][Ni(mnt)$_2$] arises from the spin-lattice interactions. The further investigations were done for the crystal structure, magnetic susceptibility and heat capacity of [NO_2-Py][Au_xNi_{1-x}(mnt)$_2$] (x = 0.01-0.73) solid solutions, which reveal the spin-Peierls transition vanishing in the heavier doped system (x > 0.27), demonstrating that the magnetostructural phase transition in [NO_2-Py][Ni(mnt)$_2$] is the intrinsic feature of S = ½ Heisenberg AFM linear chains. β-[CN-Py][Ni(mnt)$_2$] shows the same crystal structures as that of [NO_2-Py][Ni(mnt)$_2$] with rather similar unit cell parameters in both regular chain HTP and dimerized chain LTP,[45,46] and the magnetostructural phase transition in β-[CN-Py][Ni(mnt)$_2$] arises mainly from spin-lattice interaction of magnetic chains.

Conclusion

In summary, we successfully achieved a new kinetically preferred polymorph of charge-transfer salt 1-(4-cyanobenzyl)pyridinium bis(maleonitriledithiolato)nickelate. The new polymorph shows a fascinating magnetic phase transition at ~192 K associated with a symmetry broken structure phase transition. In HTP, both anions and cations form regular stacks, respectively, and the new polymorph features

magnetically as a regular S = ½ Heisenberg AFM linear chain system. In LTP, the anion and the cation stacks are dimerized, leading to a spin gap opening with nonmagnetic ground state. As a result, the magnetic phase transition occurring in the new kinetically preferred polymorph shows the typical character of a spin-Peierls-type transition and the magnetic-lattice interactions of magnetic chains is the driving force of the magnetostructural phase transition in this spin system.

Acknowledgement

Authors thank the National Nature Science Foundation of China (Grant No. 21671100, 21271103) and the Natural Science Foundation of Jiangsu Province (Grant No. BK20170145).

Supporting Information

The Supporting Information is available free of charge at https://pubs.acs.org/doi/10.1021/acs.cgd.

Experimental and simulated PXRD profiles of α- and β-phase at room temperature, the stacking patterns of adjacent anions/cations in an anion/cation stack in HTP of β-phase, H-bond interactions between anion and cation in α-phase, DSC curve of α-phase, variable temperature AC conductivity of β-phase in 123-373 K. Crystallographic data and refinement parameters for α-phase in HTP and LTP in the literature and this work, comparison of bond lengths/angles in anion and cation between single crystal at 296 K and geometry optimization in α- and β-phase (PDF).

Accession Codes

CCDC-932830 (α-phase) and CCDC-1427934 and 1903767 (β-phase) contain the supplementary crystallographic data for this paper. These data can be obtained free of charge via www.ccdc.cam.ac.uk/data_request/cif, or by emailing data_request@ccdc.cam.ac.uk, or by contacting The Cambridge Crystallographic Data Centre, 12 Union Road, Cambridge CB2 1EZ, UK; fax: (+44) 1223-336-033.

Notes and References

1. Braga, D.; Grepioni, F.; Maini, L.; Polito, M. Crystal Polymorphism and Multiple Crystal Forms. *Struct. Bond.* **2009**, *132*, 87−95.
2. Kumar, A.; Nguyen, A. H.; Okumu, R.; Shepherd, T. D.; Molinero, V. Could Mesophases Play a Role in the Nucleation and Polymorph Selection of Zeolites. *J. Am. Chem. Soc.* **2018**, 140, 16071−16086.
3. Braun, D. E.; Vickers, M.; Griesser, U. J. Dapsone Form V: A Late Appearing Thermodynamic Polymorph of a Pharmaceutical, *Mol. Pharmaceutics* **2019**, 16, 3221−3236.
4. Wang, S.; Wang, S.; Jiang, L.; Wang, M.; Wei, Y.; Sun, J.; Zhan, S.; Li, X.; Qu, L. Polymorph-Controlled Crystallization of Acetaminophen through Femtosecond Laser Irradiation. *Cryst. Growth Des.* **2019**, 19, 3265−3271.
5. Blagden, N. Crystal Engineering of Polymorph Appearance: the Case of Sulphathiazole. *Powder Tech.* **2001**, 121, 46–52.
6. Chen, B. R.; Sun, W.; Kitchaev, D. A.; Mangum, J. S.; Thampy, V.; Garten, L. M.; Ginley, D. S.; Gorman, B. P.; Stone, K. H.; Ceder, G.; Toney, M. F.; Schelhas, L. T. Understanding Crystallization Pathways Leading to Manganese Oxide Polymorph Formation. *Nat. Commun.* **2018**, 9, 2553.
7. Bernstein, J. *Polymorphism in Molecular Crystals*, Clarendon Press: Oxford, **2002.**
8. Rodríguez-Spong, B.; Price, C. P.; Jayasankar, A.; Matzger, A. J.; Rodríguez-Hornedo, N. General Principles of Pharmaceutical Solid Polymorphism: A Supramolecular Perspective. *Adv. Drug Delivery Rev.* **2004**, 56, 241−274.
9. Davey, R. J. Pizzas, Polymorphs and Pills. *Chem. Commun.* **2003**, 1463−1467.
10. Dunitz, J. D.; Bernstein, J. Disappearing Polymorphs. *Acc. Chem. Res.* **1995**, 28, 193−200.
11. Gentili, D.; Gazzano, M.; Melucci, M.; Jones, D.; Cavallini, M. Polymorphism as an Additional Functionality of Materials for Technological Applications at Surfaces and Interfaces. *Chem. Soc. Rev.* **2019**, 48, 2502−2517.
12. Avendano, C.; Zhang, Z. Y.; Ota, A.; Zhao, H. H.; Dunbar, K. R. Dramatically

Different Conductivity Properties of Metal–organic Framework Polymorphs of Tl(TCNQ): An Unexpected Room-Temperature Crystal-to-Crystal Phase Transition. *Angew. Chem. Int. Ed.* **2011**, 50, 6543−6547.

13. Duan, H. B.; Chen, X. R.; Yang, H.; Ren, X. M.; Xuan, F.; Zhou, S. M. Disorder–order Transformation and Significant Dislocation Motion Cooperating with a Surprisingly Large Hysteretic Magnetic Transition in a Nickel-bisdithiolene Spin System. *Inorg. Chem.* **2013**, 52, 3870−3877.
14. Chen, X. R.; Ning, W. H.; Yang, H.; Liu, J. L.; Xuan, F.; Ren, X. M. Observation of Hysteretic Magnetic Phase Transitions Coupled with Orientation Motion of Ions and Dielectric Relaxation in a One-dimensional Nickel-bis-dithiolene Molecule Solid. *Dalton Trans.* **2014**, 43, 6251−6261.
15. Mills, M. B.; Wohlhauser, T.; Stein, B.; Verduyn, W. R.; Song, E.; Dechambenoit, P.; Rouzières, M.; Clérac, R., Preuss, K. E. Magnetic Bistability in Crystalline Organic Radicals: the Interplay of H-bonding, Pancake Bonding, and Electrostatics in 4-(2′-Benzimidazolyl)-1,2,3,5-dithiadiazolyl. *J. Am. Chem. Soc.* **2018**, 140, 16904−16908.
16. Li, T.; Tan, G. W.; Shao, D.; Li, J.; Zhang, Z. C.; Song, Y.; Sui, Y. X.; Chen, S.; Fang, Y.; Wang, X. P. Magnetic Bistability in a Discrete Organic Radical. *J. Am. Chem. Soc.* **2016**, 138, 10092−10095.
17. Jeannin, O.; Clérac, R.; Fourmigué, M. Order-disorder Transition Coupled with Magnetic Bistability in the Ferricinium Salt of a Radical Nickel Dithiolene Complex. *J. Am. Chem. Soc.* **2006**, 128, 14649−14656.
18. Kahn, O.; Martinez, C. J. Spin-transition Polymers: from Molecular Materials toward Memory Devices. *Science* **1998**, 279, 44−48.
19. Peierls, R. E. *Quantum Theory of Solids* (Oxford University Press, London, England, **1955**, p.108−114.
20. Bray, J. W.; Hart, H. R.; Interrante, Jr. L. V.; Jacobs, I. S.; Kasper, J. S.; Watkins, G. D.; Wee, S. H.; Bonner, J. C. Observation of a Spin-Peierls Transition in a Heisenberg Antiferromagnetic Linear-Chain System. *Phys. Rev. Lett.* **1975**, 35, 744−747.

21. Pouget, J.-P.; Foury-Leylekian, P.; Almeida, M. Peierls and Spin-Peierls Instabilities in the $Per_2[M(mnt)_2]$ Series of One-Dimensional Organic Conductors; Experimental Realization of a 1D Kondo Lattice for M = Pd, Ni and Pt. *Magnetochemistry* **2017**, 3, 13(1−24).
22. Henriques, R. T.; Alcacer, L.; Pouget, J. P.; Jérome, D. Electrical Conductivity and X-ray Diffuse Scattering Study of the Family of Organic Conductors $(perylene)_2M(mnt)_2$, (M = Pt, Pd, Au). *J. Phys. C: Solid State Phys.* **1984**, 17, 5197–5208.
23. Gama, V.; Henriques, R. T.; Almeida, M.; Pouget, J.-P. Diffuse X-ray Scattering Evidence for Peierls and 'spin-Peierls' Like Transitions in the Organic Conductors $(Perylene)_2M(mnt)_2$ [M = Cu, Ni, Co and Fe]. *Synth. Met.* **1993**, 55–57, 1677–1682.
24. Huizinga, S.; Kommandeur, J.; Sawatzky, G. A.; Thole, B. T.; Kopinga, K.; de Jonge, W. J. M.; Roos, J. Spin-Peierls Transition in N-Methyl-N-ethylmorpholinium-ditetracyanoquinodimethanide [MEM-$(TCNQ_2)$]. *Phys. Rev. B* **1979**, 19, 4723–4732.
25. Tsuchiizu, M.; Sugiura, M.; Suzumura, Y. Quantum Phase Transition between the Spin-Peierls State and the Antiferromagnetic State in the TMTTF Organic Compounds. *Physica B* **2005**, 358, 42–49.
26. Nakazawa, Y.; Sato, A.; Seki, M.; Saito, K.; Hiraki, K.-i.; Takahashi,T. Spin-Peierls Transition of the Quasi-one-dimensional Electronic System $(DMe\text{-}DCNQI)_2M$ (M = Li, Ag) Probed by Heat Capacity. *Phys. Rev. B* **2003**, 68, 085112.
27. Jeannin, O.; Reinheimer, E. W.; Foury-Leylekian, P.; Pouget, J.-P.; Auban-Senzier, P.; Trzop, E.; Colletc, E.; Fourmigué, M. Decoupling Anion-ordering and Spin-Peierls Transitions in a Strongly One-dimensional Organic Conductor with a Chessboard Structure, $(o\text{-}Me_2TTF)_2NO_3$. *IUCrJ* **2018**, 5, 361–372.
28. Hase, M.; Terasaki, I.; Uchinokura, K. Observation of the Spin-Peierls Transition in Linear Cu^{2+} (Spin-1/2) Chains in an Inorganic Compound $CuGeO_3$, *Phys. Rev.*

Lett. **1993**, 70, 3651−3654.

29. Seidel, A.; Marianetti, C. A.; Chou, F. C.;Ceder, G.; Lee1, P. A. S = 1/2 Chains and Spin-Peierls Transition in TiOCl, *Phys. Rev. B* **2003**, 67, 020405(R).
30. Law, J. M.; Hoch, C.; Glaum, R.; Heinmaa, I.; Stern, R.; Kang, J.; Lee, C.; Whangbo, M.-H.; Kremer, R. K. Spin-Peierls Transition in the S = ½ Compound $TiPO_4$ Featuring Large Intrachain Coupling. *Phys. Rev. B* **2011**, 83, 180414(R).
31. Xie, J. L.; Ren, X. M.; He, C.; Song, Y.; Meng, Q. J.; Kremer, R. K.; Yao, Y. G. Complicated Magnetic Behavior in One-dimensional Nickel(III) Chain Complex [1-(4'-cyanobenzyl)pyridinium][Ni(mnt)$_2$] (mnt^{2-} = Maleonitriledithiolate). *Chem. Phys. Lett.* **2003**, 369, 41−48.
32. Davison, A.; Holm, R. H. Metal Complexes Derived from Cis-1, 2-dicyano-1, 2-ethylenedithiolate and Bis(trifluoromethyl)-1, 2-dithiete. *Inorg. Synth.* **1967**, 10, 8−26.
33. Software packages SMART and SAINT, Siemens Analytical X-ray Instrument Inc., Madison, WI, **1996**.
34. Sheldrick, G. M. Crystal Structure Refinement with SHELXL. *Acta Cryst.* **2015**, C71, 3−8.
35. Spek, A. L. Structure Validation in Chemical Crystallography. *Acta Cryst.* **2009**, D65, 148−155.
36. Segall, M. D.; Lindan, P. J. D.; Probert, M. J.; Pickard, C. J.; Hasnip, P. J.; Clark, S. J.; Payne, M. C. First-principles Simulation: Ideas, Illustrations and the CASTEP code. *J. Phys.: Condens. Matter* **2002**, 14, 2717−2744.
37. Milman, V.; Winkler, B.; White, J. A.; Pickard, C. J.; Payne, M. C.; Akhmatskaya, E. V.; Nobes, R. H. Electronic Structure, Properties, and Phase Stability of Inorganic Crystals: A Pseudopotential Plane-wave Study. *Int. J. Quantum Chem.* **2000**, 77, 895−910.
38. Perdew, J. P.; Burke, K.; Ernzerhof, M. Generalized Gradient Approximation Made Simple. *Phys. Rev. Lett.* **1996**, 77, 3865−3868.
39. Notes: As shown in Figure S5, the Ni(1) atom locates at a general site, its two neighbors Ni(1)#1 and Ni(1)#2 atoms in an anion stack are generated via the

symmetric transforms #1 = x, 0.5-y, -0.5+z and #2 = x, 0.5-y, 0.5+z. If the fractional coordinates of Ni(1) is defined as (x, y, z), then two neighbors Ni(1)#1 and Ni(1)#2 have the fractional coordinates of (x, 0.5-y, -0.5+z) and (x, 0.5-y, 0.5+z), respectively. The distances of Ni(1)…Ni(1)#1 and Ni(1)…Ni(1)#2 are correspondingly equal to the moduli of the vectors of (0, 0.5-2y, -0.5) and (0, 0.5-2y, 0.5). Obviously, the vectors of (0, 0.5-2y, -0.5) and (0, 0.5-2y, 0.5) locate on the YZ-plane of the crystallographic coordinate system. Since two-dimensional coordinate system (Y-O-Z) is orthogonal in the monoclinic system, the lengths of the vectors should be given by $|Ni(1)...Ni(1)\#1| = |(0, 0.5-2y, -0.5)| = \{0^2 + (0.5-2y)^2 + (-0.5)^2\}^{1/2}$ and $|Ni(1)...Ni(1)\#2| = |(0, 0.5-2y, 0.5)| = \{0^2 + (0.5-2y)^2 + (0.5)^2\}^{1/2} = \{0^2 + (0.5-2y)^2 + 0.5^2\}^{1/2}$. Thus, |Ni(1)...Ni(1)#1| = |Ni(1)...Ni(1)#2|, moreover, the distance of Ni(1)#1...Ni(1)#2 = |Ni(1)#1...Ni(1)#2| = |(0, 0, 1)|, namely, the Ni(1)#1...Ni(1)#2 distance is equal to the crystallographic cell length of *c*-axis.

40. Tian, Z. F.; Ren, X. M.; Li, Y. Z.; Song, Y.; Meng, Q. J. A New Quasi-1D Spin System with Spin Transition Exhibiting Novel CN…π Interactions. *Inorg. Chem.* **2007**, 46, 8102−8104.
41. Bonner, J. C.; Fisher, M. E. Linear Magnetic Chains with Anisotropic Coupling. *Phys. Rev. A* **1964**, 140, 640−658.
42. Hall, J. W.; Marsh, W. E.; Weller, R. R.; Hatfield, W. E. Exchange Coupling in the Alternating-chain Compounds Catena-μ_2-chloro-bis(4-methylpyridine)copper(II), Catena-μ_2-bromobis(N-methylimidazole)copper(II), Catena-[hexanedione bis(thiosemicarbazonato)]copper(II), and Catena[octanedione Bis(thio-semicarbazonato)]copper(II). *Inorg. Chem.* **1981**, 20, 1033−1037.
43. Tucker, D. A.; White, P. S.; Trojan, K. L.; Kirk, M. L.; Hatfield, W. E. Identification of a Novel Tetragonally Compressed Six-coordinate Copper(II) Complex: Preparation and Characterization of a 3-Chloroanilinium Copper Chloride Complex, (3-chloroanilinium)$_8$[CuCl$_6$]Cl$_4$. *Inorg. Chem.* **1991**, 30, 823−826.

44. Vasil'ev, A. N.; Markina, M. M.; Popova, E. A. Spin Gap in Low-dimensional Magnets. *Low Temp. Phys.* **2005**, 31, 203−223.

45. Ren, X. M.; Meng, Q. J.; Song, Y.; Lu, C. S.; Hu, C. J.; Chen, X. Y. Unusual Magnetic Properties of Oone-dimensional Molecule-based Magnets Associated with a Structural Phase Transition. *Inorg. Chem.* **2002**, 41, 5686−5692.

46. Ren, X. M.; Akutagawa, T.; Noro, S.; Nishihara, S.; Nakamura, T.; Yoshida, Y.; Inoue, K. Structural and Magnetic Investigations for the Doping Effect of Nonmagnetic Impurity on the Spin-Peierls-like Transition in a Quasi-one-dimensional Magnet: 1-(4'-nitrobenzyl)pyridinium Bis(maleonitrile-dithiolato)nickelate. *J. Phys. Chem. B* **2006**, 110, 7671−7677.

For Table of Contents Use Only

A new kinetically preferable polymorph of 1-(4'-cyanobenzyl)pyridinium bis(maleonitriledithiolato)nickelate with spin-Peierls type transition

Guo-Jun Yuan, Dong-Sheng Shao, Qiu Ren, Fei-Yan Feng, Hao Yang, Lifeng Wang, Xiao-Ming Ren

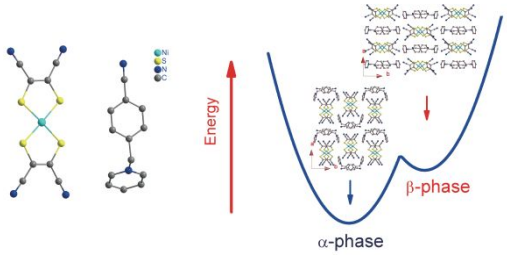

The unpredictably achieved β-phase polymorph of 1-(4'-cyanobenzyl)pyridinium bis(maleonitriledithiolato)nickelate is kinetically preferred and exhibits a spin-Peierls type transition.